Nanolamellar magnetoelectric $BaTiO_3-CoFe_2O_4$ bicrystal

Shenqiang Ren,[1] Mark Laver,[2] and Manfred Wuttig[1,a)]
[1]*Department of Materials Science and Engineering, University of Maryland, College Park, Maryland 20742-2115, USA*
[2]*NIST Center for Neutron Research, Gaithersburg, Maryland 20899-6103, USA*

(Received 30 July 2009; accepted 9 September 2009; published online 13 October 2009)

Here, we report a spontaneously formed nanolamellar $BaTiO_3-CoFe_2O_4$ bicrystal. $(1\bar{1}0)$ interfaces join the $BaTiO_3$ and $CoFe_2O_4$ single crystalline periodically arranged lamellae that have a common [111] direction. The superlattice of approximately 2 nm wavelength is magnetoelectric with a frequency dependent coupling coefficient of 20 mV/Oe cm at 100 Hz. The $BaTiO_3$ component is a ferroelectric relaxor with a Vogel–Fulcher temperature of 311 K. The relaxor behavior gives rise to a magnetic tunability of the relative dielectric constant $\langle\varepsilon_r\rangle^{-1}d\varepsilon_r/dH\approx 10^{-2}$. Since the material can be produced by standard ceramic processing methods, the discovery represents great potential for magnetoelectric devices. © *2009 American Institute of Physics*. [doi:10.1063/1.3241999]

Recently, an impressive revival of studies on magnetoelectricity has occurred. Preparation of a material in which ferroelectricity and ferromagnetism coexist in a single crystal at room temperature would present a milestone for modern electronics and functional materials. However, single phase ferroelectric ferromagnets are rare,[1] exhibit cryogenic ferroic transition temperatures, and have weak magnetoelectric coupling. Therefore, strain coupled composites of the two materials are currently technologically more interesting. Here, we report on a naturally grown nanoperiodic bicrystal in which single crystalline lamellae of ferromagnetic $CoFe_2O_4$ (CFO) and ferroelectric $BaTiO_3$ (BTO) components are epitaxially joined. The Curie temperatures of both components lie above room temperature and the coupling constant is larger than of any single phase material known.

The phase separation at nanoscopic length scales in chemically homogeneous complex oxide systems and the resulting multifunctionality is a research area of growing interest in both fundamental science and application oriented technology.[2,3] Solid-state self-assembly is an especially intriguing approach that has been used recently to form regular morphologies on a nanoscale in a series of perovskite or spinel solid solutions, which phase separate to form pseudoperiodic chessboardlike structures with promising potential functionalities.[4–6] We used this approach to improve on previous eutectoid[7] and other[8–11] syntheses of CFO/BTO composites. Avellaneda and Harshe[12] already demonstrated that solidification of eutectic BTO-CFO leads to lamellar microstructures. Phase separated self-assembled BTO/CFO three-dimensional nanostructures are also formed in pulsed laser deposited films.[12] Despite the elegance of this method, economically motivated efforts are continuing[12] to synthesize magnetoelectric composites by conventional ceramic processing. However, the resulting micro or nanostructural control is generally unsatisfactory. Here, we present an approach of preparing a periodic two-dimensional lamellar BFO/CFO nanostructure that persists throughout entire crystal grains. We have discovered that the quinary system Fe-Co-Ti-Ba-O spontaneously phase separates into a superlattice of epitaxially joined ferromagnetic CFO and ferroelectric BTO nanolamellae. This remarkable structure is mediated by the framework of oxygen octahedra that dictates the extraordinary perfection of the CFO/BTO superlattice. Compared to recent reports on other multiferroics,[13] this spontaneous phase separated perovskite-spinel system is unique in many respects; it is a naturally grown nanolamellar bicrystal with a large initial ferromagnetic susceptibility and at the same time a ferroelectric relaxor permitting large magnetoelectric tunability.

Powders of BTO-CFO (1:1 ratio) were prepared by a modified PECHINI sol-gel synthesis[14] and long time (24 h) annealed at 1473 K. X-ray diffraction and electron elemental line scan characterization show two sets of features matching with the perovskite and spinel phases and consistent with the phase diagram of the quinary system Fe–Co–Ti–Ba–O.[12] The corresponding nanometer scale transmission electron microscopy (TEM) images (Fig. 1) display two types of contrast at different length scales. Figure 1(a) displays the low magnification TEM contrast whose periodicity is identical to that of the nanolamellae seen in Fig. 1(b). This figure exhibits a periodic arrangement of layers with an average spacing of less than 2 nm. It will be seen that the layers consist of alternating CFO and BTO lamellae. The BTO layers contain a dark center line that is only visible at certain orientations. It represents a hexagonal stacking fault in the three unit BTO cell layer. The Rietveld analysis of the x-ray data indicates the presence of 50%CFO, 25% cubic, and 25% hexagonal BTO, i.e., a 50/50 mixture of cubic and hexagonal BTO. This apparent oddity is resolved by the stacking fault in the BTO layer; since the BTO lamella contains only three lattice units the hexagonal fault occupies 50% of its volume. The x-ray data also indicate a c/a ratio of the hexagonal portion of 2.4 in agreement with known data.[15]

High magnification TEM images representative 50%CFO/50%BTO crystals and their corresponding diffraction patterns are shown in Fig. 1(c), which shows details of the lamellar structure. The measured unit supercell is consistent with the periodicities determined from the XRD Rietvield analysis. Further confirmation of the phase separation is seen in the elemental mapping imaged at high resolution TEM. Selected area electron diffraction patterns of the superlattice taken along the $\langle 111\rangle$ zone axis [see inset of Fig. 1(c)]

a)Electronic mail: wuttig@umd.edu.

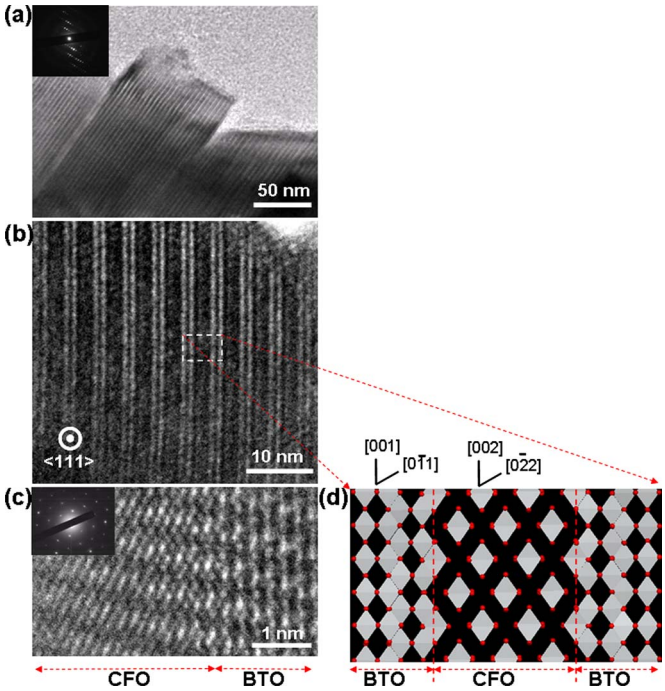

FIG. 1. (Color online) (a) Low magnification image including a selected area electron diffraction pattern demonstrating the long coherence length of the periodic structure. (b) Conventional image; the dark and bright areas are CFO and BTO lamellae, respectively, and the dark center line in the bright stripes is the image of a stacking fault. (c) [111] zone HRTEM images showing the atomic structure of each layer of the bicrystal. (d) Schematic diagram of the in-plane image corresponding to the common ⟨111⟩ zone axis. The oxygen octahedra appear as rhombes. It shows the stacking fault in the BTO portion and the corrugated interface at which oxygen octahedra "belonging" to CFO and BTO overlap.

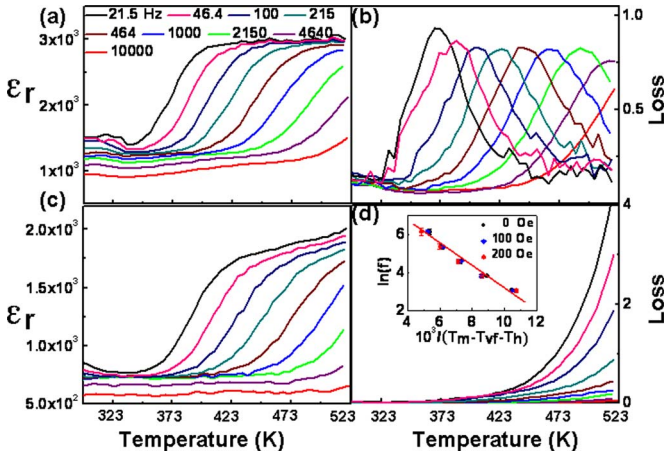

FIG. 2. (Color online) [(a) and (b)] Relative dielectric constant and loss factor vs temperature measured at different frequencies. [(c) and (d)] Relative dielectric constant and loss factor vs temperature of the bicrystal when subjected to an external magnetic field of 100 Oe. The inset of image (d) demonstrates the Arrhenius behavior of the frequency of the loss maximum at the temperature, T_m, validating the Vogel–Fulcher relationship in different magnetic fields, h=0, 100, and 200 Oe.

indicate the formation of the crystalline cubic phases. Materials studio simulations of the boundary region gave optimum matching for a simple $3a_p$ perovskite and $2a_s$ spinel one-dimensional supercell [Fig. 1(d)], $a_{p,s}$ are the perovskite and spinel lattice parameters, which together represent a single period of the BTO-CFO bicrystal oriented perpendicularly to the ⟨111⟩ axis. This arrangement also agrees with the stoichiometry of the sample. The low and high resolution TEM images and compositional data in their entirety thus suggest that the lamellar nanostructure consists of three faulted unit cells perovskite BTO and two unit cells spinel CFO meaning, equivalently, that nanometer-scale phase separation has occurred. It is accommodated by the low energy $(1\bar{1}0)$ interface. The oxygen octahedra at the BTO/CFO interfaces are hexagonally arranged and some oxygen octahedra overlap, i.e., the interface is corrugated, see Fig. 1(d).

It is known that the decomposition of an amorphous or nanocrystalline CFO/BTO solid solution in a magnetic field results in a periodic nanostructure reminiscent of a spinodal decomposition into two cubic phases.[14] The present decomposition at high temperatures likely occurs via a pseudospinodal process[16] during which a periodic structure of CFO and BTO (Ref. 17) is formed first. The stacking fault then represents the remainder of the hexagonal phase after it is transformed to the low temperature cubic modification under constraint upon cooling. The resulting epitaxial stress in CFO is given by $\sigma_{110}^{CFO}=Y^{CFO}\varepsilon_{110}^{epi}$, $\varepsilon_{110}^{epi}=(d_{220}^{CFO}-d)_{110}^{BTO}/\left[\left(\frac{1}{2}\right)(d_{220}^{CFO}+d_{110}^{BTO})\right]$, whereas the stored epitaxial elastic energy $U_{111}=\frac{1}{2}(\varepsilon_{110}^{epi})^2Y^{CFO/BTO}$. The quantity $Y^{CFO/BTO}$ is the shear modulus of the CFO/BTO parallel composite. With the values Y^{BTO}=67 GPa (Ref. 18) and Y^{CFO}=141.6 GPa,[19] $U_{111}=4.7\times10^6$ J/m^3. This elastic energy is significantly lower than $U_{100}=2.7\times10^7$ J/m^3 observed in thin films of the same system.[14] The small epitaxial strain also leads to a small magnetoelastic energy density of $CoFe_2O_4$, $U_{mel}=[(\lambda_{100}^{CFO}+3\lambda_{111}^{CFO})/4]\varepsilon_{110}^{epi}Y^{CFO}=-1.67\times10^5$ J m^{-3}. λ represents the magnetostriction coefficients of CFO.[19]

The ferroelectric properties of the BTO/CFO two-dimensional nanosuperlattice are equally interesting. Normally, BTO is a typical ferroelectric crystal. However, according to the temperature and frequency dependencies of the dielectric constant, ε_r, and loss factor, see Fig. 2, as part of the present composite it is a relaxor ferroelectric[20,21] characterized by a Vogel–Fulcher temperature T_{VF}=311 K. The dielectric response depends on the external magnetic field as shown clearly in Figs. 2(c) and 2(d). Note that, for example, the relative dielectric constant at f=21.5 Hz equals 2250 but decreases to 800 if a field of 100 Oe is applied at 400 K, i.e., a remarkable magnetic tunability $\langle\varepsilon_r\rangle^{-1}d\varepsilon_r/dH\approx10^{-2}$. Information about the nature of the clusters,[22] thought to cause relaxor behavior, can be extracted from the activation enthalpy of the Vogel–Fulcher relationship, $\ln(f/f_0)=(\Delta H)/[k(T_m-T_{vf}-T_h)]$ shown in the insert of Fig. 2(d). If $\Delta H_{mel}=T_hk=8K\cdot k$ is a magnetoelastic energy density, it follows that the extent of the cluster equals approximately one perovskite lattice constant. It may thus be argued that the relaxation occurs at the CFO/BTO interface.

The zero room temperature ferromagnetic remnance of the superlattice shown in Fig. 3(a) can be understood if it is assumed that neighboring CFO layers are antiferromagnetically coupled through their dipolar interaction. This assumption is indirectly supported by Lorentz TEM observations, which did not show any indication of domain walls in the remnant state. The initial steep rise of the magnetization is determined by the magnetization rotation in the CFO sheet plane. The initial susceptibility, χ_i, will then be determined by the balance of the magnetic and effective anisotropy energy densities of CFO, $\chi_i=(I_s^{CFO})^2/[2(K_u^{CFO}+U_{mel})]$. The quantities I_s and K_u designate the saturation magnetization

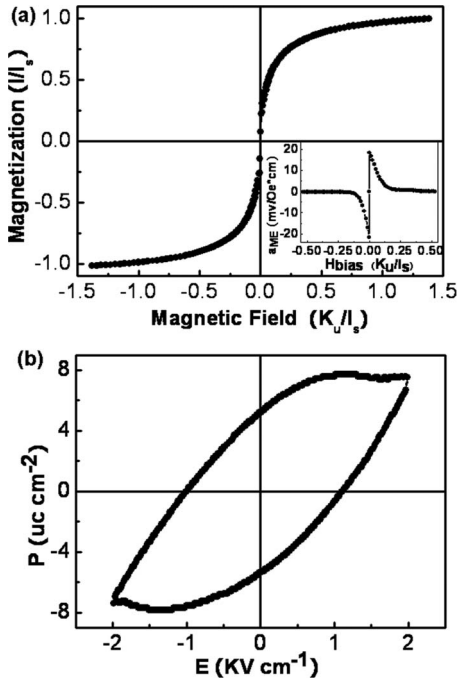

FIG. 3. (a) Room temperature magnetic hysteresis loop, the right-hand figure shows the magnetoelectric coupling constant, α_{ME}, determined with a magnetic ac field of 100 Hz as a function of the normalized magnetic bias field, the maximum occurs at a bias field of 10 Oe. (b) Polarization loop at room temperature.

and magnetocrystalline anisotropy energy densities, respectively. Since $K_u^{CFO}=2\times10^5$ J m^{-3} (Ref. 23) and $U_{mel}=-1.7\times10^5$ J m^{-3} (see above) the rotational susceptibility is much larger than that of unconstrained single crystalline CFO. The approach to saturation of the sheets is governed by the total anisotropy field o.o. $[K_u^{CFO}+U_{mel}+(I_s^{CFO})^2]/(I_s^{CFO})$,[24] i.e., saturation would be achieved much more gradually as the magnetization components now rotate against the demagnetization field. The normalized plot of the experimental data confirms these expectations.

The CFO/BTO nanobicrystal is naturally magnetoelectric at room temperature as the components' critical temperatures are higher than it. The magnetoelectric coupling constant of a sample consisting of randomly oriented CFO/BTO platelets displays a maximum of $\alpha_{ME}=20$ mV/cm Oe at the extremely small dc bias magnetic field of 10 Oe. This constant is larger than those displayed by any natural magnetoelectric crystal. The inset of Fig. 3(a) displays the field dependence of the coupling constant. The electric field induced polarization (P-E) behavior is shown in Fig. 3(b). The BTO-CFO compound exhibits well saturated hysteresis loops with a remnant polarization (P_r) and the coercive field (E_c) of about 11 μC/cm^2 and 1 kV/cm, respectively. The observed P_r value is higher than the reported value of polycrystalline BTO ceramics.[25]

Periodicities with the level of perfection we report here have not, to our knowledge, ever been observed in multiferroic perovskite-spinel self-assembled nanostructures. The {111} orientation appears to provide the lowest energy interfacial configurations for perovskite-spinel systems. The coexistence of relaxor ferroelectricity and magnetic order[26] has attracted considerable attention due to their peculiar properties and various applications.[27] We have already shown that within one homologous solid solution, the periodic phase separated perovskite-spinel superlattice can be synthesized. By varying the compositional ratio and introducing chemical substitutes, it should be possible to improve on one or more of many technologically important functionalities in the combined perovskite and spinel families.

This work was supported by NSF (Grant No. DMR0705368), ONR-MURI (Grant No. N000140110761), ARO-MURI (Grant No. 28D1083899), UMD-MRSEC, and UMD-Nanocenter program, for permission to use its equipment.

[1] M. Fiebig J. Phys. D: Appl. Phys. **38**, R123 (2005).
[2] V. S. Stubican and A. H. Schultz, J. Am. Ceram. Soc. **51**, 290 (1968).
[3] H. U. Habermeier, J. Phys.: Condens. Matter **20**, 434228 (2008).
[4] B. S. Guiton and P. K. Davies, Nature Mater. **6**, 586 (2007).
[5] S. Garcia-Martin, E. Urones-Garrote, M. C. Knapp, G. King, and P. M. Woodward, J. Am. Chem. Soc. **130**, 15028 (2008).
[6] S. Yeo, Y. Horibe, S. Mori, C. M. Tseng, C. H. Chen, A. G. Khachaturyan, C. L. Zhang, and S.-W. Cheong, Appl. Phys. Lett. **89**, 233120 (2006).
[7] J. Van Suchtelen, Philips Res. Rep. **27**, 28 (1972).
[8] S. Ren and M. Wuttig, Appl. Phys. Lett. **91**, 083501 (2007).
[9] J. Van Den Boomgaard, D. R. Terrell, R. A. J. Born, and H. F. J. I. Giller, J. Mater. Sci. **9**, 1705 (1974).
[10] S. Ren and M. Wuttig, Appl. Phys. Lett. **92**, 083502 (2008).
[11] H. Zheng, J. Wang, S. E. Lofland, Z. Ma, L. Mohaddes-Ardabili, T. Zhao, L. Salamanca-Riba, S. R. Shinde, S. B. Ogale, F. Bai, D. Viehland, D. G. Schlom, M. Wuttig, and R. Ramesh, Science **303**, 661 (2004).
[12] M. Avellaneda and G. Harshe, J. Intell. Mater. Syst. Struct. **5**, 501 (1994).
[13] W. Eerenstein, M. Wiora, J. L. Prieto, J. F. Scott, and N. D. Mathur, Nature Mater. **6**, 348 (2007).
[14] S. Q. Ren, L. Q. Weng, S. H. Song, and F. Li, J. Mater. Sci. **40**, 4375 (2005).
[15] R. D. Burbank and H. T. Evans, Acta Crystallogr. **1**, 330 (1948).
[16] Y. Ni and A. Khachaturyan, Nature Mater. **8**, 410 (2009).
[17] Y. Wu, S. Wang, and H. Lu, J. Am. Ceram. Soc. **89**, 3778 (2006).
[18] W. Duffy, B. Cheng, M. Gabbay, and G. Fantozzi, Metall. Mater. Trans. A **26**, 1735 (1995).
[19] V. J. Folen, *Magnetic and Other Properties of Oxides and Related Compounds*, Landolt–Börnstein, New Series, Group III, Vol. 3, Pt. B (Springer, New York, 1970).
[20] D. Viehland, J. F. Li, L. E. Cross, and M. Wuttig, Phys. Rev. B **46**, 8013 (1992).
[21] J. Hemberger, P. Lunkenheimer, R. Fichtl, H.-A. Krug von Nidda, V. Tsurkan, and A. Loidl, Nature (London) **434**, 364 (2005).
[22] L. E. Cross, Ferroelectrics **76**, 241 (1987).
[23] R. Valenzuela, *Magnetic Ceramics* (Cambridge University Press, Cambridge, 1994).
[24] S. Chikazumi, *Physics of Magnetism*, 2nd ed. (Oxford University Press, Cary, NC, 1997), p. 491.
[25] X. Wang, X. Deng, H. Wen, and L. Li, Appl. Phys. Lett. **89**, 162902 (2006).
[26] A. Kumar, G. Sharma, R. Katiyar, R. Pirc, R. Blinc, and J. F. Scott, arXiv:0812.3875v2.
[27] N. Hur, S. Park, P. A. Sharma, J. S. Ahn, S. Guha, and S.-W. Cheong, Nature (London) **429**, 392 (2004).